Computational Materials Science 188 (2021) 110183

Contents lists available at ScienceDirect

Computational Materials Science

journal homepage: www.elsevier.com/locate/commatsci

# Microstructural evolution in ZrCu metallic glass under neutron irradiation

Yi-fu Dong [a], Ming-fei Li [a], Babafemi Malomo [b], Liang Yang [a,*]

[a] College of Materials Science and Technology, Nanjing University of Aeronautics and Astronautics, Nanjing 210016, PR China
[b] Dept. of Mechanical Engineering, Obafemi Awolowo University, Ile-Ife, Nigeria

ARTICLE INFO

*Keywords:*
Molecular dynamics
Irradiation effect
Metallic glass
Defect
Self-healing

ABSTRACT

A detailed numerical investigation has been conducted on the microstructural evolution of a $Zr_2Cu$ metallic glass (MG) model under neutron irradiation by extensive molecular dynamics simulations. It was discovered that at the melted zone of the irradiated MG model, an irradiation-induced cascades region was prominent, where there exists a significant atomic-to-cluster structural changes in terms of the coordination numbers, atomic packing efficiency, cluster distribution and regularity. These features effectively were responsible for the transformation of disordered local structures from a densely-packed to a loosely-packed arrangement and largely, the underlying chaos within the structure. Eventually, it was highly remarkable to discover that when the model was fully relaxed at 20 ns, the irradiation-induced structural changes completely vanished and the entire structure was effectively and fully self-recovered. The results of this study will potentially facilitate the development of advanced materials with high irradiation resistance.

## 1. Introduction

The quest for high performance structural materials that are suitable for the design of fission and fusion reactors in nuclear energy systems has been indeed quite challenging. This is so, because such materials must meet stringent requirements in order to possess extended service life in aggressive environments where they are subject to the effects of high temperatures, elevated stress levels, chemical corrosion and high-energy irradiation, amongst others [1–5]. The most commonly found nuclear structural materials are mainly the crystalline alloys which are well-known to suffer significantly from high-energy particle irradiation and in particular, by neutron irradiation effects. The primary structural changes resulting from these, are the irradiation-induced Frenkel defects, which by their accumulation leads to macro-structural damage and performance degradations, such as: swelling, hardening, embrittlement, amorphization, etc [6,7]. Consequently, it is crucial to design and develop novel structural materials possessing high resistance to neutron irradiation and efforts to meet this critical requirement have continued to inspire extensive research interests [8]. Hitherto, high-entropy alloys and nanocrystalline materials have been considered as potential candidates of a new class of nuclear structural materials, due to their relatively stable structures and effective self-healing abilities under neutron irradiation [9–12]. In spite of this, these materials suffer structural degradation by nuclear irradiation. For instance, some residual point defects cannot be annealed in nanocrystallines and they practically transform into the microscopic entities that are either absorbed at the grain boundaries or at the surfaces [13].

As compared with crystalline alloys, metallic glasses (MGs) have excellent properties such as high strength, high hardness, and high corrosion resistance [14–17]; but unlike them, MGs are fully amorphous in nature with the tendency to eliminate irradiation-induced crystalline defects as confirmed by validation in a previous work [18]. In addition, besides the volume expansion (swelling), the volume contraction which have relatively low saturation values was observed in MGs. However, while some irradiated MGs surprisingly became even more ductile, significant irradiation-caused embrittlement was observed in almost all of the crystalline alloys [19]. The foregoing indicates that MGs could likely possess a high neutron irradiation resistance because of their unique amorphous structures. Nonetheless, it still remains a daunting challenge to experimentally investigate the structural changes in MGs due to neutron irradiation because of the following constraints: 1) the length and time scales of materials subject to damage by neutron irradiation span from the atomic (nanometer, picosecond) to the macroscopic (meter, year); 2) the microstructures of MGs are rather complex such that, experimental methods cannot provide reliable and detailed structural information unlike those found in crystalline alloys. To address these difficulties, some computational approaches have been successfully applied to investigate the microstructures of amorphous

* Corresponding author.
*E-mail address:* yangliang@nuaa.edu.cn (L. Yang).

https://doi.org/10.1016/j.commatsci.2020.110183
Received 5 September 2020; Accepted 12 November 2020
Available online 1 December 2020

alloys based on the reasoning that more detailed information on atomic-level structural changes can be captured by theoretical formulations and implemented in a robust numerical framework [20–23].

Therefore, in this current work, the structural evolution of MGs under irradiation is systematically investigated by performing a classical molecular dynamics simulation [24] in order to characterize their structural stability under neutron irradiation.

## 2. Simulation methods

### 2.1. Building an amorphous model

Zr-based alloy systems consist of a variety of compositions that have been found to possess good glass-forming abilities, making them the foremost choice and most suitable alloys for nuclear power plant applications. On this premise, a Zr-rich binary composition ($Zr_2Cu$) was selected as the research prototype in this work [25]. A classical MD was performed by the Large-scale Atomic/Molecular Massively Parallel Simulator (LAMMPS). An Embedded Atom Method (EAM) [26] interatomic potential was applied to ensure that a precise interaction between Zr and Cu atoms in both the liquid and the amorphous solid structures is established. Furthermore, the short-range part of the potential employed was smoothly joined by the Ziegler-Biersack-Littmark (ZBL) function [11]. An NPT (constant number of particles, pressure, and temperature) ensemble was applied to idealize and account for molecular conformational changes during the simulation.

Using LAMMPS, an appropriate molecular structural lattice was constructed, which is a tetragonal $Zr_2Cu$ supercell model containing 653,184 atoms. The simulation was initiated by rapidly heating the model to a temperature of 2000 K and maintaining it at that temperature for 8 ns to obtain a stable liquid $Zr_2Cu$ model. The resulting melt was quenched to 300 K at a constant cooling rate of $10^{10}$ K/s, by maintaining the external pressure at zero bar in the three coordinate directions. The quenched model was subsequently relaxed at 300 K for another 8 ns to obtain a stable as-constructed $Zr_2Cu$ amorphous model with a volumetric size of $23.4 \times 23.6 \times 23.6$ nm$^3$.

### 2.2. Simulation of collision cascades

To simulate the collision cascades phenomenon induced by neutron irradiation in MD, an 'hypothetical' Zr primary knock-on atom (PKA) was strategically positioned in the model. To ensure that PKA can produce detectable cascading collisions without penetrating the model, it is required to generate a PKA with appropriate energy [27,28]. Therefore, a Zr PKA with kinetic energy of 15 keV was selected, by using the Stopping and Range of Ions in Matter (SRIM) program [29]. The initial position and direction of travel of the PKA were set at the corner and along the diagonal of the model respectively.

As collision cascades were initiated by the PKA, chaotic collisions between various atoms led to a series of microstructural changes within the MG model. The Collision cascades process was simulated in the NVE (constant number of particles, volume, and energy) ensemble. At the end of the collision cascades event, the NVE ensemble was found inadequate to appropriately simulate the cooling process of the MG model, hence, an NPT ensemble with a constant time step of 2 fs, held over a period of 20 ns was applied for the simulation. As shown in Fig. 1, the variable step as a function of the simulation time was plotted to describe the behavior of the model simulated in the NVE ensemble. It was observed that the variable time step rose rapidly from approximately 0.10 ps to 0.85 ps, which is indicative of the period of effective collision cascades. Beyond 0.85 ps, the variable time step no longer increased, thereby signifying the onset of the post-collision cascades period.

From the curve shown in Fig. 1, some typical snapshots of the model depicting the events at the simulation times of 0 ps, 0.21 ps and 0.85 ps, corresponding to the as-constructed, the collision cascades and the transition between collision and post-collision cascades states

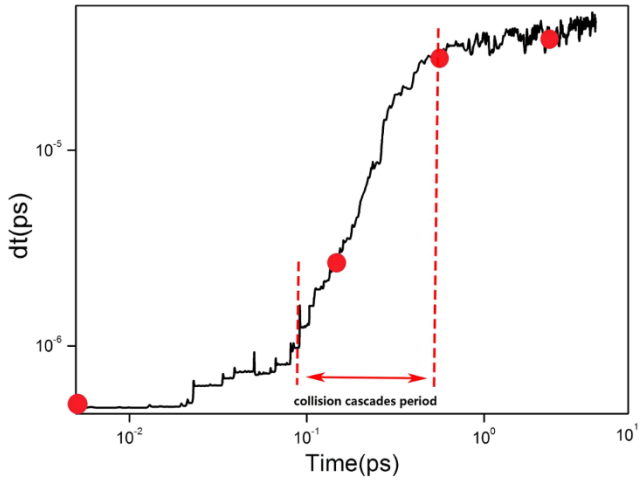


**Fig. 1.** The variable time step as a function of the simulation time for the model simulated in the NVE ensemble. Data in the NPT ensemble is not shown here.

respectively were analyzed. In line with the well-established theory that vacancy-like defects could be annihilated in the post-collision cascades [30], a snapshot of the model at 4.27 ps was also selected along with that of 20 ns denoting the period at which full structural relaxation is complete. From the analysis of the structural features given by the selected five snapshots, it was feasible to evaluate the microstructural evolution characteristics of the MG model during the MD simulations.

It has been reported that apart from the knocked-on atoms in the collision cascades region, other microscopic events, such as the free volumes and vacancy-like excrescencies certainly evolve in an amorphous model. Hence, it was crucial to thoroughly analyze the collision cascades region. To identify the zone where the collision cascades took place in the MG model, all the knocked-on Cu and Zr atoms whose kinetic energies were greater than 0.8 eV, were selected and shown in Fig. 2(a). Because 0.8 eV kinetic energy is much larger than that caused by the thermal equilibrium, it would be considered as an excessive kinetic energy to set the atoms in motion [30]. The OVITO software program was implemented [31] for the simulation and observation details. From thence, it was apparent that the collision cascades phenomena only occurred within a local region of the model. A typical representation of this region is shown as highlighted in Fig. 2(b), which was estimated at a region approximately 1/27 of the entire model. To justify the collision cascades effect, an arbitrary region of equal size adjacent to the collision cascades region as shown in Fig. 2(b) was selected to pinpoint the variation.

During the simulation, the melting point ($T_m$) of the $Zr_2Cu$ model was approximately 1800 K [11], and the melted region induced by the collision cascades was estimated according to the relations;

$$E_k = \frac{3k_B T_m}{2} \tag{1}$$

where $E_k$ is the atomic kinetic energy and $k_B$, the Boltzmann constant. The melting threshold $E_k$ value was recorded as 0.234 eV and all atoms possessing kinetic energies greater than 0.234 eV were selected. In this way, the liquid-like region could be estimated. The liquid-like region is an irregular three-dimensional space. Therefore, a regular cube with a small size of $3 \times 3 \times 3$ nm$^3$ was cut out of the liquid-like region and shown in Fig. 2(b). This region was considered to have been fully melted during the collision cascades period. It was discovered that the melted zone was filled up with high-energy atoms and as a result, it was significantly active and its influence dominant in the collision cascades region. Although the region was primarily referred to as a liquid-like region, but the collision cascades-induced melt ultimately transformed into a solid after quenching and subsequent relaxation of the structure. To provide an insightful information on this

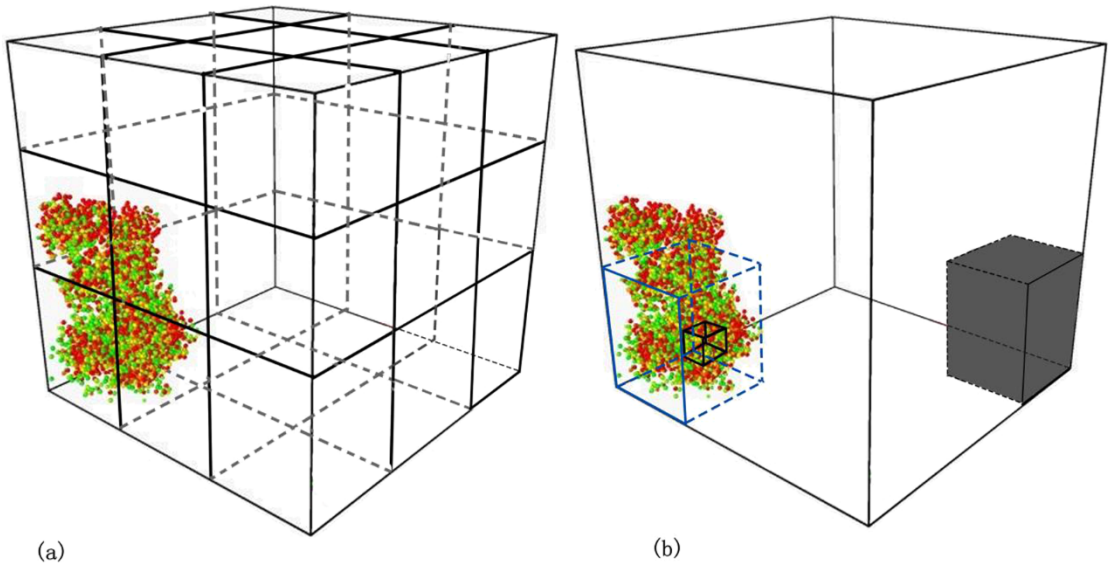


**Fig. 2.** Spatial distribution of knocked-on atoms with a kinetic energy higher than 0.8 eV in (a) collision cascades model, and (b) the highlights of collision cascades region (blue dashed cube), liquid-like region (black solid cube), and a cubic region adjacent to the collision cascades (shaded cube).

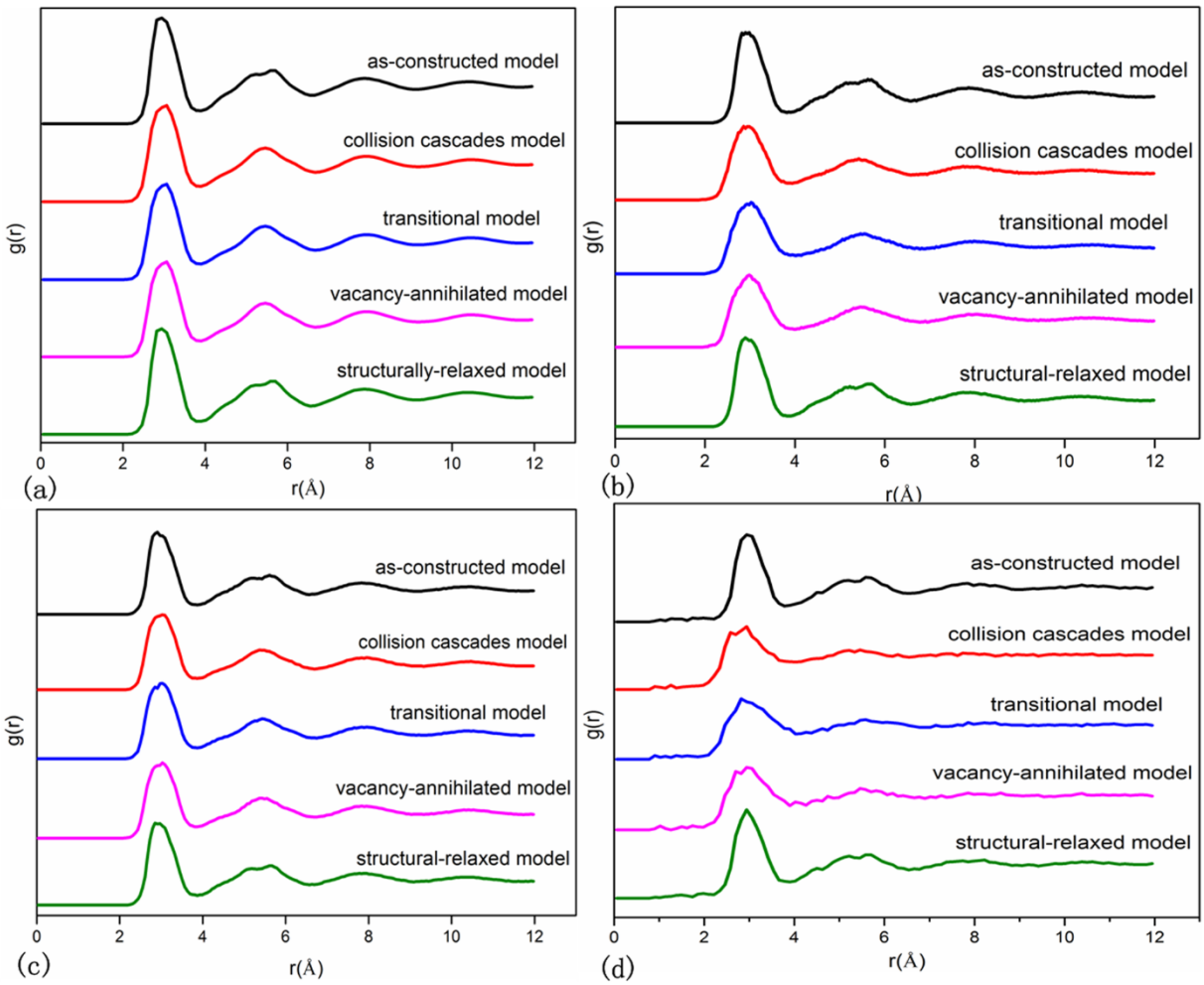


**Fig. 3.** g(r) vs r(Å) plots at selected regions of the five snapshots representing (a) the entire model, (b) the collision cascades region, (c) the non-collision cascades region, and (d) the liquid-like region.

behavior; the phenomena of structural evolution in the collision cascades region, the non-collision cascades region and the melted region were compared during the MD simulations.

To closely investigate the structural evolution by MD simulation in this work, some salient and specific MG structural parameters or features [25,30,32,33], such as the radial distribution function (RDF), coordination numbers (CNs), cluster distributions, cluster regularity ($T$ value), and atomic packing efficiency, were studied.

## 3. Results and discussion

### 3.1 Radial distribution function (RDF)

RDF describes how atomic density varies as a function of the distance $r$ from a reference particle. It can be calculated by the expression [34]

$$g(r) = \frac{V}{N}\left\langle \sum_{i=1}^{N} \frac{n(r)}{4\pi^2 \Delta r} \right\rangle \quad (2)$$

where $N$ is the number of atoms, $V$ represents the volume of the system, and $n(r)$ denotes the number of particles found within the shell from $r$ to $r + \Delta r$. The RDF curves of the total $Zr_2Cu$ model from the five snapshots of Fig. 1 are shown in Fig. 3(a). It can be readily observed from the plots that there were broad and smooth first-, second-, third-, and fourth-shell peaks, in the $r$ range from 2.0 to 11.8 Å of the as-constructed model, and these features invariably classify it as a fully amorphous structure [25]. Nonetheless, it's remarkable to note that, regardless of the aforementioned representations being replicated as characteristics of the snapshots (1st to 4th shell peaks) for the collision cascades, transitional model, and vacancy-annihilated models which invariably also denote them as fully amorphous structures; the noticeable variations in the RDF curves in terms of the peak intensity and width, clearly suggest that there were certain unusual structural changes in the entire model during irradiation. This is evident, specifically by the split-in-peak pattern of the second shell which clearly signifies that the relatively ordered packing in amorphous solid is non-existent forthwith. Be that as it may, the RDF curve of the structurally-relaxed model is almost similar to the as-constructed one and this clearly indicates an effective self-healing behavior of the $Zr_2Cu$ amorphous model.

Fig. 3(b)–(d) are the RDF curves of the collision cascades region, the non-collision cascades region, and the liquid-like region of the five snapshots, respectively. The figures altogether clearly indicate the impressions of noticeable structural changes. On this basis, it is highly objective to assert in regard to the three intermediate snapshots of the liquid-like region with the exception of the first-shell peak, that no apparent peak features were detected in other distribution shells. This potentially implies that the "short-to-medium range" orders which essentially are the well-known intrinsic structural features in an amorphous solid, were probably annihilated when the regions were irradiated. Nevertheless, multiple-shell peaks surprisingly reappear in the structurally-relaxed snapshot, in a similar manner as compared with those of the as-constructed model. This in effect clearly suggests that in spite of the fact that many disordered local structures induced by irradiation exist in the liquid-like region, their effective recovery can be achieved upon the structural relaxation of the amorphous model. This is tenable because the liquid-like region is active within the collision cascades region and therefore, the order-to-disorder-to-order transformation chain in the liquid-like zone strongly influenced the structural change in the collision cascades region. At which point, some disordered local structures appeared during irradiation such indicated by the intensity and width of the distribution peaks that decreased and increased, respectively. With reference to the non-collision cascades region which is located considerably away from the collision cascades, the structure remained largely unchanged.

### 3.2. Coordination numbers (CNs)

The CN is a parameter that denotes the neighborhood of a central atom which was determined in this study by calculation via a custom-built Voronoi-tessellation program developed in-house. To determine or calculate the CN parameter in a large model is mostly considered a time-consuming and error-prone endeavor, therefore the emphasis here was to focus on the determination of the CN parameter for the five snapshots by strictly limiting the investigation to the collision cascades region, the non-collision cascades region and the liquid-like region. For the as-constructed model snapshot, the major CN values were found to lie within the range of 11–15 with an average value of 13. This indicates that the atoms are more likely to be centered in some densely-packed [35] local structures which usually contains more than 12 shell atoms. Furthermore, it is quite remarkable to observe from the structurally-relaxed snapshot that, the CN values of all the three regions were almost similar in representations to those from the same regions of the as-constructed snapshot. This remarkably confirms that regardless of the structural changes induced by the collision cascades, effective recovery from the deterioration would be achieved when the microstructures of MGs are fully relaxed. Considering the transitional region snapshot, the CN parameter was observed to sharply reduce to a minimal value of 11.6, which consequently is a factor indicating the transition from a densely-packed local structure constitution to a relatively loosely-packed one in the melted region. This behavior largely occurred because the liquid-like region was dominant in the collision cascades zone which is a plausible inference by virtue of the reduction in CN parameter recorded for the transitional snapshot. However, there were no significant variations of the CN values at the non-collision cascades region during the simulation, thereby suggesting that the model structure was largely stable within this region.

### 3.3. Distribution and regularity of Voronoi clusters (VCs)

Amorphous solids, especially MGs are composed of specific structural units generally referred to as clusters. These clusters can be geometrically indexed by the Voronoi tessellation method [36,37] and are critical to understanding the structural behavior of MGs. Therefore, it was highly crucial to analyze clusters evolution during the MD simulation of the $Zr_2Cu$ model. This was carried out by extracting major VCs from the collision cascades region, the non-collision cascades region, and the liquid-like region, and their respective graphical distributions are as shown in Fig. 5. It could be readily inferred from the pictorial representations that the distributions of all the major clusters were similar in both the as-constructed and structurally-relaxed

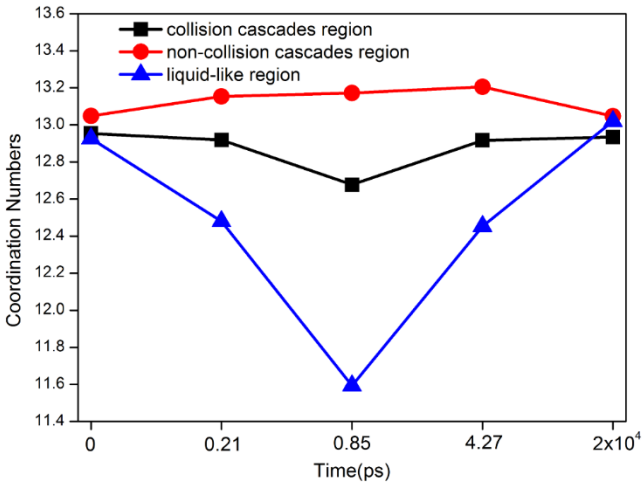


**Fig. 4.** CNs of five snapshots in different regions.

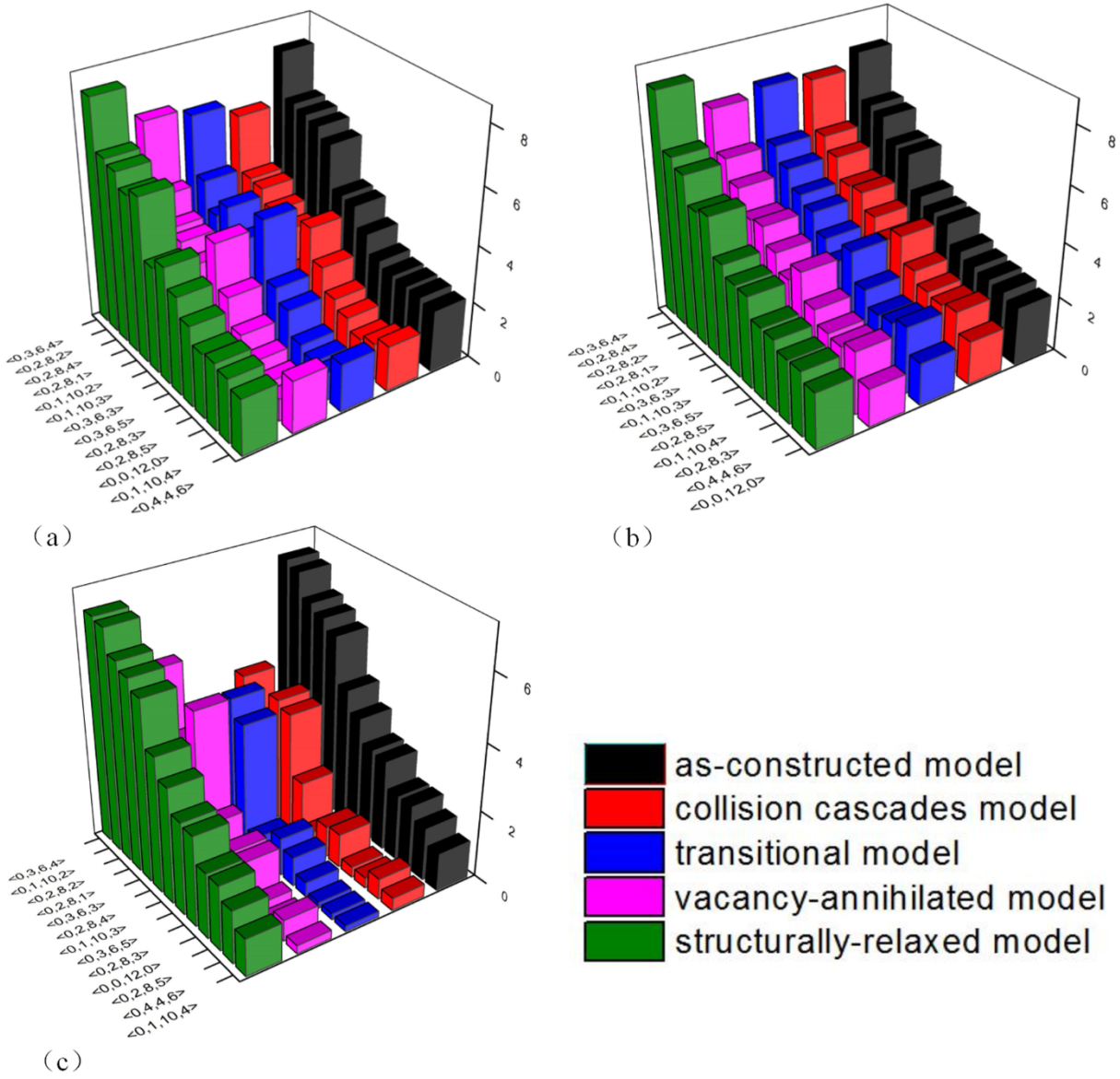


**Fig. 5.** The plot of the distributions of VCs in five snapshots, at (a) the collision cascades region, (b) the non-collision cascades region, and (c) the liquid-like region.

snapshots, which indicate at the cluster level, an effective self-healing mechanism of the structures. This observation is quite consistent with the performances of g(r) and CN as discussed in the previous section.

Furthermore, by investigating the liquid-like region of the model, it was noticed that majority of the major VCs were depleted and replaced by minor-type VCs during the MD simulation. This phenomenon compels a plausible deduction that the short-range order of the amorphous solid was annihilated by the collision cascades, such that the arrangement of atoms now become rather more randomly distributed within the melt. In spite of the aforementioned, it was interestingly unusual to discover that, as the distributions of some distorted icosahedral VCs, of $< 0,2,8,1 >$ and $< 0,3,6,3 >$ increased on one hand; the other icosahedral ($<0,0,12,0>$) or distorted icosahedral VCs, of $< 0,2,8,2 >$ and $< 0,1,10,2 >$ decreased. Specifically, the $< 0,2,8,1 >$ and $< 0,3,6,3 >$ VCs are the relatively loosely-packed or the low 5-fold symmetrical local structures, while the $< 0,0,12,0>$, $<0,2,8,2,>$, and $< 0,1,10,2 >$ VCs are the full densely-packed or the high 5-fold symmetrical icosahedral clusters [37]. This intrinsic characteristic behavior indicates that regardless of the rich and abundant icosahedral-like clusters present in the melt in comparison with the as-prepared amorphous solid [38] most of the clusters are loosely-packed and not densely-packed structures. It may be further elicited that the high cluster-level change in the liquid-like region was responsible for the relatively small variation in the collision cascades region. Furthermore, it was apparent that there were no cluster changes in the non-collision cascades region where the structure is considered to be largely stable during the simulation.

A crucial aspect of the foregoing analysis is to determine the Voronoi index, strictly by the rotational symmetries of shell atoms in each cluster [39], hence, there is no need to consider the cluster regularity and to account for the effects of bond lengths, bond angles, and chemical fluctuation of atoms, in the formulations. By reason of the fact that each VC is made up of a number of Delaunay tetrahedra points sharing a common vertex (the center atom in a VC); clusters can adjust their geometric regularities without modifying their Voronoi indices due to the low energy barrier to be subdued [40,41]. Therefore, the regularity of the entire VC could be estimated by calculating the regularity of each tetrahedron. In this work, a parameter of tetrahedral degree ($T$) was adopted to predict a deviation from the regular tetrahedron [42]:

$$T = \sum_{i=j} (e_i e_j)^2 / 15\langle e \rangle^2 \tag{3}$$

where $e$ is the length of the i-th side, $<e>$ is the average of the

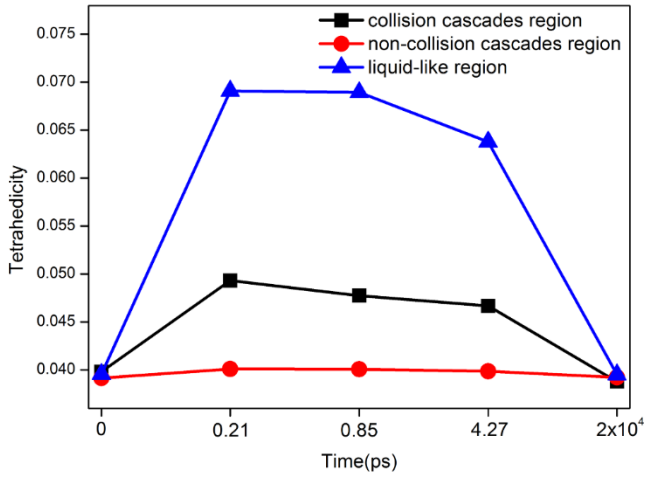


**Fig. 6.** The regularity plots of five snapshots at different regions.

tetrahedron six sides. When $T$ is zero, the tetrahedron is considered a regular one. The larger the $T$ value, the more irregular the tetrahedra and the corresponding VCs would be. The relationships between the $T$ values and simulation periods were plotted and presented in Fig. 6.

During the simulation, the $T$ value for the liquid-like region sharply increased from 0.04 to approximately 0.07, which is a trend indicating that the regularities of the tetrahedra and corresponding VCs were quickly modified with a potential tendency to be more irregular. The change in $T$ values is in tandem and profoundly consistent with the phenomenon that had been previously reported, specifically regarding how "the short-range order was annihilated such that the densely-packed clusters were easily transformed into loosely-packed ones at the irradiation-induced melted zone". This behavior confirms that random-packing of atoms in local structures is responsible for the underlying chaos within the system and not by the influence of order characteristics defined in terms of bond lengths, bond angles and chemical fluctuations. The variation in $T$ values also occurred in the collision cascades region but this effect was not detected in the non-collision cascades region. Nonetheless, it was observed that the $T$ values increased and attained a value of 0.04 following a trend similar to the behavior of the as-constructed snapshot upon quenching the model to room temperature and after the full relaxation of its structure. This manifestation further confirms an earlier disclosure that an MG model can effectively and fully self-recover when its structure is fully relaxed.

### 3.4. Atomic packing efficiency (APE)

As it has been revealed from previous analysis of the model characteristics, that certain changes of local structures are associated with the collision cascades, particularly in the liquid-like region, it follows that the changes in the distribution and regularity of clusters could probably have occurred due to the constraint of a more random atomic-packing arrangement; this notwithstanding, an inclusive description of atomic packing during the simulation remains largely unknown. To circumvent this challenge and provide insightful information, a theoretical parameter (APE) which can indicate the extent of dense-atomic packing in clusters that is also related to glass-forming events in alloys, has been proposed [43,44]. The APE values ($\eta$) for the models investigated in this study were determined by a method illustrated in a previous work [25], according to the relations;

$$\eta = \frac{V_a}{V_u} \tag{4}$$

where $V_a$ and $V_u$ denote the volume of the embedded atoms in a cluster and the total volume of the cluster respectively. $V_u$ can be obtained by summing the volumes of all the VCs with the associated tetrahedra, since each VC was built by stacking myriads of tetrahedra onto a shared vertex positioned at the VC's center atom's location. Therefore, based on the concept that each atom embedded in the cluster is truncated as a cone ball, it follows that by adding the volumes of all the cone balls, $V_a$ is determined. The relationships between the APE values and the simulation period were plotted and presented in Fig. 7. It can be readily inferred that the $\eta$ value of the as-constructed snapshot is approximately 0.68 which is equivalent to that of a BCC crystalline phase.

This interpretation is plausible and quite reasonable because the microstructures of MGs are known to present short-to-medium range order characteristics where atoms are rather densely-packed. From the plots, it was notably unusual to observe that the $\eta$ value in the liquid-like region sharply decreased during the simulation to as low as 0.60 for the transitional snapshot. This invariably implies that the atoms were quite loosely-packed and this peculiarity is certainly responsible for the presence of more loosely-packed and irregular clusters for the transitional snapshot as indicated in Figs. 4–6. However, when irradiation induced defects were healed and the structure fully relaxed, the $\eta$ values increased and attained approximately the same value of the as-constructed state. The evolution of the $\eta$ values in collision cascades region is similar to their representations in the liquid-like region, while those for the region adjacent to the collision cascades, remained constant. The foregoing analysis uniquely validates the effective self-healing behavior in irradiated MGs.

### 3.5. Self-healing mechanism

With reference to the totality of all the structural parameters and features investigated in this study, such as; the RDFs, CNs, distribution and regularity of VCs, and the APE, it is feasible to evaluate how the structure of an MG model responds to irradiation. Basically, irradiation imparted a collision cascade region in the $Zr_2Cu$ model where high-kinetic energy atoms are concentrated causing a thermal spike effect [45] and consequently, a melted local region. At the melted region, the intrinsic short-to-medium range in an amorphous solid is destroyed, such that atoms now become more randomly and loosely-packed, triggering a molecular chaos. As a consequence, broader atomic distribution peaks appeared in the RDF curves, densely-packed clusters with large CNs transformed to loosely-packed structures with small CNs and clusters became more irregular in geometry. Consequently, short-to-medium range order was sustained in the region adjacent to the collision cascades, prompting the occurrence of structural instability and energy imbalances within the entire model. Eventually, it was found that the melted region quenched at a very fast cooling rate of $10^{12}$ K/s, a

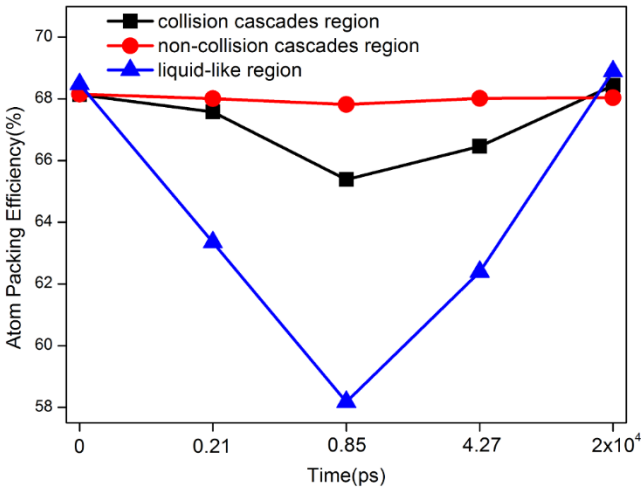


**Fig. 7.** APE of five snapshots in different regions.

performance that is consistent with the super-quench phenomenon reported in a previous work [45]. This behavior is attributed to the fact that the melted zone is a relatively small region of the model surrounded by amorphous regions where the short-to-medium range order was well-preserved under irradiation. These conditions strategically promoted a structural rejuvenation effect in the melted region. In other words, when the structure of the melted region was fully relaxed, the RDF peaks, CNs, distribution and regularity of VCs, as well as the APE values were transformed into those observed for the as-constructed state. This ultimately indicates that the MG material model possesses a highly effective and an impressive full self-recovery ability when subjected to irradiation damage and this performance is at variance with the behavior of the so-called crystalline alloys.

## 4. Conclusion

A systematic and insightful investigation on the microstructural evolution of a $Zr_2Cu$ MG model under neutron irradiation effects has been performed by molecular dynamics simulation, and the following deductions were drawn from the study.

1. It was discovered that the collision cascades region which is a local region of the model was significantly affected by irradiation, leading to an irradiation-induced melted zone.
2. The melted zone is characterized by a highly disordered structure due to the concentration of high-energy atoms as compared with the neighboring amorphous solid region, which is a manifestation of the influence of an active mechanism that aided the effective transformation from dense-packing to loosed-packing local structures.
3. Upon the full structural relaxation of the entire model after the melted zone was rapidly and spontaneously quenched, all irradiation-induced structural changes instantaneously became insignificant. This scenario establishes the effective self-healing ability of the amorphous alloy model.
4. The performance characteristics of the structural parameters and features investigated, such as; the RDFs, CNs, distribution and regularity of VCs, and the APE factors have provided a methodical framework to evaluate the response of an MG structure to irradiation; hence the results of this study provide a novel scheme to aid the synthesis and selection of candidate nuclear materials with high irradiation resistance.

## Declaration of Competing Interest

The authors declare that they have no known competing financial interests or personal relationships that could have appeared to influence the work reported in this paper.

## Acknowledgements

Financial supports from the National Natural Science Foundation of China (Grant No. 51471088) and the Fundamental Research Funds for the Central Universities (Grant No. NE2015004), are gratefully acknowledged.

## References

[1] S.J. Zinkle, J.T. Busby, Structural materials for fission & fusion energy, Mater. Today. 12 (2009) 12–19.
[2] S.J. Zinkle, G.S. Was, Materials challenges in nuclear energy, Acta Mater. 61 (2013) 735–758.
[3] R. Prăvălie, G. Bandoc, Nuclear energy: Between global electricity demand, worldwide decarbonisation imperativeness, and planetary environmental implications, J. Environ. Manage. 209 (2018) 81–92.
[4] D.J. Hill, Nuclear energy for the future, Nat. Mater. 7 (2008) 680–682.
[5] Y. Guérin, G.S. Was, S.J. Zinkle, Materials challenges for advanced nuclear energy systems, MRS Bull. 34 (2009) 10–19.
[6] K.E. Sickafus, R.W. Grimes, J.A. Valdez, A. Cleave, M. Tang, M. Ishimaru, S. M. Corish, C.R. Stanek, B.P. Uberuaga, Radiation-induced amorphization resistance and radiation tolerance in structurally related oxides, Nat. mater. 6 (2007) 217–223.
[7] T.D.D.L. Rubia, H.M. Zbib, T.A. Khraishi, B.D. Wirth, M. Victoria, M.J. Caturla, Multiscale modelling of plastic flow localization in irradiated materials, Nature 406 (2000) 871–874.
[8] E. Francis, R.P. Babu, A. Harte, T.L. Martin, P. Frankel, D. Jädernäs, J. Romero, L. Hallstadius, P.A.J. Bagot, M.P. Moody, M. Preuss, Effect of Nb and Fe on damage evolution in a Zr-alloy during proton and neutron irradiation, Acta Mater. 165 (2019) 603–614.
[9] T. Nagase, P.D. Rack, J.H. Noh, T. Egami, In-situ TEM observation of structural changes in nano-crystalline CoCrCuFeNi multicomponent high-entropy alloy (HEA) under fast electron irradiation by high voltage electron microscopy (HVEM), Intermetallics 59 (2015) 32–42.
[10] T. Nagase, T. Hosokawa, K. Takizawa, Y. Umakoshi, Electron-irradiation-induced nano-crystallization in quasicrystal-forming Zr-based metallic glass, Intermetallics 17 (2009) 657–668.
[11] F. Xiong, M.F. Li, B. Malomo, Y. Liang, Microstructural evolution in amorphous-nanocrystalline ZrCu alloy under neutron irradiation, Acta Mater. 182 (2020) 18–28.
[12] M. Sadeghilaridjani, A. Ayyagari, S. Muskeri, V. Hasannaeimi, R. Salloom, W. Y. Chen, S. Mukherjee, Ion irradiation response and mechanical behavior of reduced activity high entropy alloy, J. Nucl. Mater. 529 (2019), 151955.
[13] X.M. Bai, A.F. Voter, R.G. Hoagland, M. Nastasi, B.P. Uberuaga, Efficient annealing of radiation damage near grain boundaries via interstitial emission, Science 327 (2010) 1631–1634.
[14] L. Lang, Z.A. Tian, S.F. Xiao, H.Q. Deng, B.Y. Ao, P.H. Chen, W.Y. Hu, Molecular dynamics simulations of the structure evolutions of Cu-Zr metallic glasses under irradiation, Nucl. Instrum. Methods Phys. Res. Sect. B Beam Interact. Mater. Atoms 393(2017) 77-81.
[15] C.A. Schuh, T.C. Hufnagel, U. Ramamurty, Mechanical behavior of amorphous alloys, Acta Mater. 55 (2007) 4067–4109.
[16] M.M. Trexler, N.N. Thadhani, Mechanical properties of bulk metallic glasses, Prog. Mater. Sci. 55 (2010) 759–839.
[17] K. Hashimoto, What we have learned from studies on chemical properties of amorphous alloys, Appl. Surf. Sci. 257 (2011) 8141–8150.
[18] W.L. Johnson, Bulk glass-forming metallic alloys: Science and technology, MRS Bull. 24 (1999) 42–56.
[19] R. Raghavan, K. Boopathy, R. Ghisleni, M.A. Pouchon, U. Ramamurty, J. Michler, Ion irradiation enhances the mechanical performance of metallic glasses, Scripta. Mater. 62 (2010) 462–465.
[20] M. Faruq, A. Villesuzanne, G. Shao, Molecular-dynamics simulations of binary Pd-Si metal alloys: Glass formation, crystallisation and cluster properties, J. Non-Cryst. Solids. 487 (2018) 72–86.
[21] L.H. Shi, Q. Li, H.M. Duan, W.B. Zhang, W.M. Yang, H.X. Li, C.T. Chang, The correlation between mechanical properties and structure of Fe-Ni-PB amorphous alloys: Ab initio molecular dynamics simulations, J. Non-Cryst. Solids. 491 (2018) 1–6.
[22] Y.S. Yun, B.J. Kim, J.H. Na, H.S. Nam, P.R. Cha, W.T. Kim, D.H. Kim, The effect of enthalpy of mixing on the atomic level structure and plasticity of amorphous alloys: A molecular dynamics simulation study in a binary model system, Intermetallics 92 (2018) 25–35.
[23] C.H. Wang, K.Chi. Chao, T.H. Fang, I. Stachiv, S.F. Hsieh, Investigations of the mechanical properties of nanoimprinted amorphous Ni–Zr alloys utilizing the molecular dynamics simulation, J. Alloys Compd. 659(2016) 224-231.
[24] S.J. Plimpton, Fast parallel algorithms for short-range molecular dynamics, J. Comput. Phys. 117 (1995) 1–19.
[25] L. Yang, G.Q. Guo, L.Y. Chen, C.L. Huang, T. Ge, D. Chen, P.K. Liaw, K. Saks, Y. Ren, Q.S. Zeng, B. LaQua, F.G. Chen, J.Z. Jiang, Atomic-scale mechanisms of the glass-forming ability in metallic glasses, Phys. Rev. Lett. 109 (2012), 105502.
[26] Y.Q. Cheng, E. Ma, H.W. Sheng, Atomic level structure in multicomponent bulk metallic glass, Phys. Rev. Lett. 102 (2009), 245501.
[27] N. Sekimura, Primary knock-on atom energy dependence of cascade damage formation and interaction, J. Nucl. Mater. 233 (1996) 1080–1084.
[28] Z.G. Cui, C.J. Gou, Q. Hou, L. Mao, Computer simulation of radiation damage caused by low energy neutron in zirconium, Acta. Phys. Sin. 62 (2013) 156105.
[29] J.F. Ziegler, M.D. Ziegler, J.P. Biersack, SRIM–The stopping and range of ions in matter, Nucl. Instrum. Methods Phys. Res. Sect. B Beam Interact. Mater. Atoms 268 (2010) 1818-1823.
[30] Y.F. Wang, H.Y. Li, Y. Liang, Radiation-induced structural evolution in $Zr_2Cu$ metallic glass, J. Mater. Sci. 53 (2018) 10979–10986.
[31] A. Stukowski, Visualization and analysis of atomistic simulation data with OVITO–the Open Visualization Tool, Modell. Simul. Mater. Sci. Eng. 18 (2009), 015012.
[32] X.D. Wang, X.C. Ren, R.T. Qu, Z.F. Zhang, Compression-compression fatigue behavior of a Zr-based metallic glass with different free volume contents, J. Alloys Compd. 810 (2019), 151924.
[33] S.K. Sharma, P.K. Pujari, Role of free volume characteristics of polymer matrix in bulk physical properties of polymer nanocomposites: A review of positron annihilation lifetime studies, Prog. Polym. Sci. 75 (2017) 31–47.
[34] G. Duan, D.H. Xu, Q. Zhang, G.Y. Zhang, T. Cagin, W.L. Johnson, W.A. Goddard, Molecular dynamics study of the binary $Cu_{46}Zr_{54}$ metallic glass motivated by experiments: Glass formation and atomic-level structure, Phys. Rev. B 71 (2005), 224208.

[35] D.B. Miracle, The efficient cluster packing model – An atomic structural model for metallic glasses, Acta Mater. 54 (2006) 4317–4336.
[36] S.Y. Wang, M.J. Kramer, M. Xu, S. Wu, S.G. Hao, D.J. Sordelet, K.M. Ho, C.Z. Wang, Experimental and ab initio molecular dynamics simulation studies of liquid $Al_{60}Cu_{40}$ alloy, Phys. Rev. B 79 (2009), 144205.
[37] G.Q. Guo, S.Y. Wu, S. Luo, L. Yang, Detecting structural features in metallic glass via synchrotron radiation experiments combined with simulations, Metals 5 (2015) 2093–2108.
[38] S. Trady, A. Hasnaoui, M. Mazroui, Atomic packing and medium-range order in $Ni_3Al$ metallic glass, J. Non-Cryst. Solid. 468 (2017) 27–33.
[39] G. Voronoi, Nouvelles applications des paramètres continus à la théorie des formes quadratiques, J. Reine. Angew. Math. 134 (1908) 198–287.
[40] X.K. Xi, L.L. Li, B. Zhang, W.H. Wang, Y. Wu, Correlation of atomic cluster symmetry and glass-forming ability of metallic glass, Phys. Rev. Lett. 99 (2007), 095501.
[41] T. Takagi, T. Ohkubo, Y. Hirotsu, B.S. Murty, K. Hono, D. Shindo, Local structure of amorphous $Zr_{70}Pd_{30}$ alloy studied by electron diffraction, Appl. Phys. Lett. 79 (2001) 485–487.
[42] N.N. Medvedev, Y.I. Naberukhin, Shape of the delaunay simplices in dense random packings of hard and soft spheres, J. Non-Cryst. Solid. 94 (1987) 402–406.
[43] D.B. Miracle, A structural model for metallic glasses, Nat. Mater. 3 (2004) 697–702.
[44] D. Turnbull, Under what conditions can a glass be formed, Contemp. Phys. 10 (1969) 473–488.
[45] R.E. Baumer, M.J. Demkowicz, Radiation response of amorphous metal alloys: Subcascades, thermal spikes and super-quenched zones, Acta Mater. 83 (2015) 419–430.